PERGAMON

Acta mater. Vol. 47, No. 9, pp. 2619–2632, 1999

Printed in Great Britain
PII: S1359-6454(99)00142-1
1359-6454/99 $20.00 + 0.00

PEARLITE TO AUSTENITE TRANSFORMATION IN AN Fe–2.6Cr–1C ALLOY

D. V. SHTANSKY†[1]‡§, K. NAKAI[2] and Y. OHMORI[2]

[1]Department of Materials Science, The University of Tokyo, 7-3-1 Hongo, Bunkyo-ku, Tokyo 113-8656, Japan and [2]Department of Materials Science and Engineering, Faculty of Engineering, Ehime University, 3 Bunkyo-cho, Matsuyama 790-8577, Japan

(Received 16 February 1999; accepted 29 April 1999)

Abstract—The mechanism of austenite formation, the kinetics of cementite lamellae dissolution and the crystallography of the austenitization from pearlite have been studied in an Fe–2.6 wt% Cr–0.96 wt% C alloy. Austenite grains nucleate after rather long incubation time both at pearlite colony boundaries and at the ferrite/cementite interfaces within a pearlite. Characteristic morphologies of transformation products were observed at various stages of transformation. Particular attention was paid to the structural evolution close to the α/γ interfaces. No indications of the diffusion ahead of the α/γ interface were found. The kinetics of austenite growth is controlled initially by carbon diffusion but in later stages by chromium diffusion. The results are discussed by assuming local equilibrium at the moving interfaces with the software and database ThermoCalc. The method involves the driving force determination for the diffusion of carbon and substitutional element during austenitization. The orientation relationships between ferrite, martensite and cementite were also determined. The possible austenite orientations were evaluated assuming the α/θ, α/γ and γ/θ orientation relationships so far obtained. © *1999 Acta Metallurgica Inc. Published by Elsevier Science Ltd. All rights reserved.*

Keywords: Phase transformations; Crystallography; Microstructure; Transmission electron microscopy (TEM); Phase diagrams

1. INTRODUCTION

Although the theory of pearlite reaction has been studied quite intensively, little attention has been given to the reverse transformation which occurs during heating. The current understanding about this reaction is mainly based on the experimental and theoretical results by Speich and Szirmae [1] who studied the austenite formation in an Fe–0.96C alloy and a plain carbon steel. They reported that nucleation of austenite occurs instantaneously at pearlite colony boundaries and the growth is controlled by carbon diffusion. At high temperatures, the growth rate of austenite will be extremely rapid. They also found that the addition of alloying elements decreases the transformation rate, but were not able to identify the mechanism of this effect. Hillert *et al.* [2] extended the theory for alloy steels and showed that the reaction may be controlled by the diffusion of substitutional elements at temperatures below some critical point. The theoretical predictions at high temperatures are not in keeping with the experimental results. In order to test the validity of these theoretical treatments, additional experiments are needed. Although a lot of literature about the austenite formation in low-carbon dual-phase steels [3–10] and low-carbon low-alloy steels [11–13] is available, the pearlite to austenite transformation has not been examined in detail. In most research it has just been noted that austenite grains grow rapidly into pearlite until the pearlite dissolution is completed.

The morphology and crystallography of grain boundary precipitates have intensively been studied [11, 14, 15], but little information is available about the crystallography of the austenitization from pearlite grains. In Fe–C–M alloys where the solute M is one of the carbide stabilizers, carbide lamellae may be retained almost undissolved even at the stage where the $\alpha \longrightarrow \gamma \longrightarrow \alpha'$ transformation is completed [16]. In such a situation, an austenite grows as lamellae within pearlite and their habit planes are fixed by carbide lamellae. Four phases form during the reaction and the question whether there exist any relationships between them arises. To answer this question, further study has to be made.

The detailed investigation of the mechanism and the crystallography of austenite formation from

†On leave from the I. P. Bardin Iron and Steel Industry Institute, 2nd Baumanskaya Street, 9/23, Moscow 107005, Russia.

‡New address: *The University of Tokyo*, Engineering Research Institute, School of Engineering, 2-11-16 Yayoi, Bunkyo-ku, Tokyo 113-8656, Japan.

§To whom all correspondence should be addressed.

both $\alpha + M_7C_3$ and $\alpha + M_{23}C_6$ pearlites in an Fe–8% Cr–C alloy has recently been presented by Shtansky *et al.* [16]. In the present study transmission electron microscopy was used to reveal the crystallography and the structural evolutions during the $(\alpha + M_3C)$ pearlite to austenite transformation in an Fe–2.6% Cr–0.95% C steel. The experimental results will be discussed quantitatively in terms of the theoretical predictions assuming the reaction to be diffusion controlled and local equilibrium to be maintained at the moving interface.

2. EXPERIMENTAL PROCEDURE

The chemical composition of the alloy used in the present investigation is shown in Table 1. Specimens of 20 mm in diameter and 10 mm long were austenitized at 1150°C for 15 min in a dynamic argon atmosphere and then cooled with an average rate of 20°C/min. Sheets $10 \times 10 \times 0.3\ mm^3$ in size were sliced from the center of each heat-treated cylinder, were finally austenitized in a salt bath at different temperatures in the range of 800–900°C for various times between 3 and 20 s, and then quenched into iced brine. Thin foils for TEM studies were prepared from 3 mm disks ground to a thickness of about 0.06 mm from both sides to remove outer layers and electropolished by a conventional twin-jet polishing method using an electrolyte containing 10% perchloric acid, 20% glycerol and 70% ethanol. The foils were examined in a JEM-3010 transmission electron microscope operating at 300 kV.

3. EXPERIMENTAL RESULTS

3.1. Initial pearlite

The initial structure consisted of lamellar pearlite with an average interlamellar spacing of about 0.1 μm. Neither proeutectoid cementite nor grain boundary ferrite was observed. The detailed examination of the pearlitic crystallography was undertaken in connection with a recent paper by Zhang and Kelly [17] who reported four new orientation relationships (ORs) between pearlitic ferrite and cementite but suggested that the widely accepted Pitsch–Petch OR [18, 19] is questionable.

The present results showed that the Pitsch–Petch OR is predominant in the alloy investigated (13 cases). The ferrite habit plane always deviated about 1.5–2° from $(001)_C//(\bar{2}\bar{1}5)_F$ that agrees well with the results of Zhou and Shiflet [20]. The angle between $[010]_C$ and $[131]_F$ was determined to be within the range of 1–3°. Thus the Pitsch–Petch OR is just an ideal approximation. Since the $(\bar{1}03)_C$ plane is parallel to $(\bar{1}01)_F$ in the case of the Pitsch–Petch OR, the New-5 OR reported by Zhang and Kelly [17] is close to the Pitsch–Petch OR.

In three cases, the Isaichev OR [21] was obtained:

$$(101)_C//(21\bar{1})_F\text{-habit plane } (0\bar{1}0)_C//(1\bar{1}1)_F.$$

This OR is fulfilled with high accuracy, and also shows good fit on the close packed $(103)_C//(110)_F$ planes. The results obtained correlate well with the conclusion of Sukhomlin [22] and Ridley [23] that the Pitsch–Petch (predominant one) and Isaichev ORs are characteristic of pearlite with eutectoid composition. For the sake of completeness, it should be noted that some peculiar relationships were occasionally observed in pearlite, i.e.

$$\begin{array}{lll} (01\bar{1})_C//(1\bar{1}0)_F\text{-habit plane} & \text{or} & (001)_C//(\bar{1}12)_F \\ (\bar{1}00)_C//(113)_F & & (0\bar{1}0)_C//(13\bar{1})_F \\ & & [110]_C\text{-habit plane normal} \end{array}.$$

The first of them is close to the New-3 OR reported by Zhang and Kelly [17] although the habit plane has not been reported. Since both of them have never been confirmed by other researchers they are probably anomalous ORs in view of the fact that the ferrite in pearlite can polygonize [24], and/or the austenite could well recrystallize due to transformation strains [25].

3.2. Nucleation of austenite

The austenite nucleation was found to occur in the specimen heated for 8 s at 800°C. Several specimens have been examined carefully after holding for 7 s at 800°C, but the austenite has never been found. According to the calculations with the software ThermoCalc [26], the composition of the alloy falls into the middle part of the $\gamma + M_3C + M_7C_3$ three-phase area at this temperature. First austenite nucleated at a pearlite colony boundary and grew only into one of the grains separated by the boundary as shown in Fig. 1(a). It should be mentioned that the austenite in the present experiment always completely transformed into martensite during the subsequent quenching. It is very useful that some part of pearlite in the right colony remained untransformed (denoted as F), thus the SAED patterns taken from the initial pearlites on either side of the grain boundary allow their crystallographic orientations to be determined. It was found that both pearlites have similar Isaichev ORs [Fig. 1(b)], the habit plane being parallel to $(\bar{1}01)_C//(\bar{1}\bar{2}1)_F$. Thus an austenite particle nucleated at a pearlite

Table 1. Chemical composition of the alloy (mass %)

C	Si	Mn	P	S	Cr	N	O	Al
0.95	0.03	0.02	0.001	0.001	2.61	0.0015	0.001	0.002

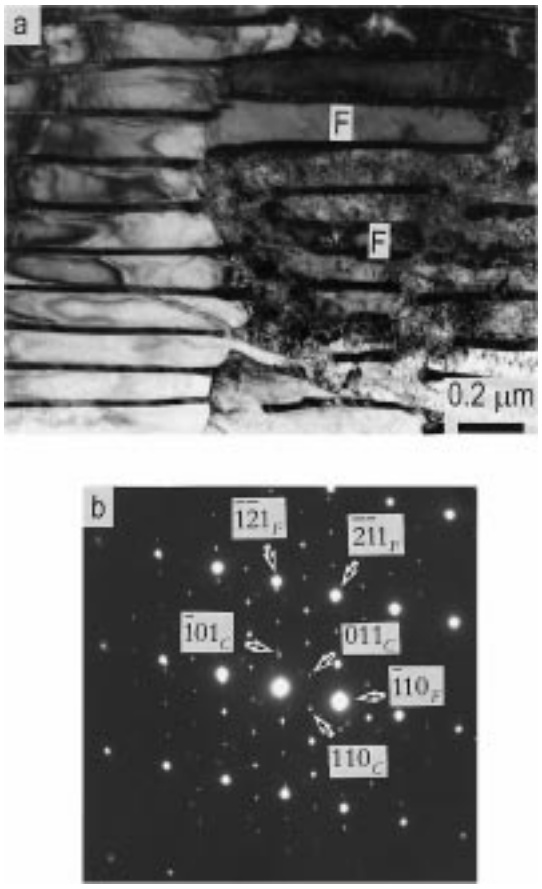

Fig. 1. (a) TEM micrograph showing the transformation of pearlite into austenite after heat treatment at 800°C for 20 s. Symbol F denotes the retained ferrite in the transformed pearlite. (b) SAED pattern showing that the initial pearlite colonies on both sides of the colony boundary possess the Isaichev OR.

colony boundary would be related to one of the pearlite constituents if it related to the same constituent in the adjacent pearlite. After $\alpha \longrightarrow \gamma \longrightarrow \alpha'$ transformation, a specific relationship between the martensite lath and the retained cementite lamellae was not found.

The $\alpha \longrightarrow \gamma$ transformation in the adjacent pearlite colony requires the independent nucleation of austenite. This is shown in Fig. 2. Two martensite regions on both sides of the grain boundary were probably formed from the different austenite grains and the initial pearlite grain boundary can easily be recognized between them.

Figure 3 shows another example of the austenite nucleation, i.e. at the ferrite/cementite interface within a pearlite. The incident beam direction is $[0\bar{1}0]_C//[113]_F$. This is the case of the Pitsch–Petch OR where the lamella habit plane is parallel to $(001)_C//(\bar{5}21)_F$. It can be seen that the carbide lamella considerably dissolved into austenite. The austenite maintains an elliptical shape until it impinges against the neighboring cementite lamellae. In this case, the austenite grain nucleated after

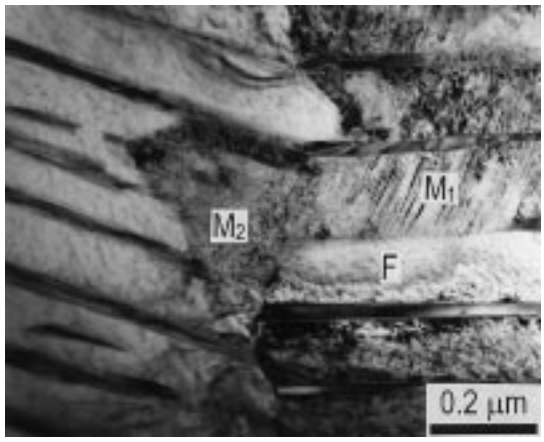

Fig. 2. TEM micrograph showing the transformation of pearlite into austenite after heat treatment at 800°C for 20 s.

rather a long time, 20 s. A similar type of nucleation was also observed in the specimen heated for much shorter time, see Fig. 6. Note that in both cases the pearlite colonies exhibited the Pitsch–Petch OR.

3.3. Growth of austenite and dissolution of cementite

After nucleation, the austenite grows within a pearlite by a diffusional process. Figures 4(a)–(d) represent various examples of the austenitization close to the α/γ interface. Figure 4(a) shows the austenite grown between two adjacent cementite lamellae. Carbide lamellae are almost undissolved in the region close to the α/γ front. It can be seen that the shape of the α/γ interface is irrational, suggesting an incoherent interface migration. Figure 4(b) shows the austenite lamella that consumed two contiguous ferrite lamellae. The cementite lamella between them was dissolving at the α/γ front, supplying carbon and substitutional atoms to the growing austenite. The cementite lamellae on both sides acted as barriers for the sidewise growth of austenite and remained almost undissolved.

Figure 4(c) shows clearly that the thickness of cementite lamella just behind the α/γ front is much reduced as shown by an arrow, suggesting the sidewise cementite dissolution. In this example, however, the austenite grains grew faster than the region where the carbide lamellae dissolved, thus cementite lamellae remained behind the α/γ front. Figure 4(d) is the case where the cementite lamellae dissolved completely just behind the moving α/γ interface.

Two specific features of the microstructural evolution should be mentioned. Figures 1(a) and 6 show that some part of the ferrite in a pearlite colony remained untransformed even after the $\alpha \longrightarrow \gamma$ transformation in the surrounding area was already completed. Another interesting case is the observation that the edges of cementite lamellae thicken and spheroidize in contact with the austenite

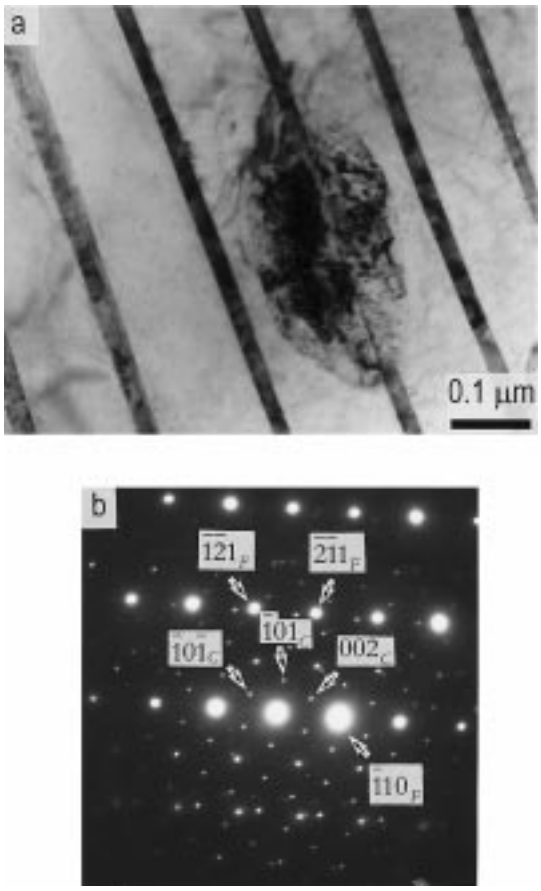

Fig. 3. (a) TEM micrograph showing the nucleation of austenite (austenite completely transformed into martensite during quenching) at the ferrite/cementite interface within a pearlite after heat treatment at 800°C for 20 s. (b) SAED pattern showing that the pearlite possesses the Pitsch–Petch OR. The incident beam direction is $[0\bar{1}0]_C//[113]_F$.

[Fig. 4(d)]. This reaction often starts at the α/γ interface and the rows of cementite particles align behind the dissolving lamella as shown in Fig. 8 (shown by arrows).

Figures 5(a) and (b) show the pearlite colony boundaries after 20 s at 800°C and 3 s at 875°C, respectively. These figures represent different stages of the α/γ transformation in two adjacent colonies. In both cases, the cementite lamellae in one of the austenite grains completely dissolved, whereas in the adjacent colony the cementite lamellae remained almost undissolved before (a) and after (b) $\alpha \longrightarrow \gamma$ transformation. In this case the austenite did not cross a pearlite grain boundary and the mark of the previous position of the grain boundary was left. Note that the edges of cementite lamellae thickened at the grain boundary.

3.4. Crystallography

The bright field (BF) image [Fig. 6(a)] and the dark field (DF) image [Fig. 6(b)] using the $(0\bar{1}1)$ ferrite reflection show the α/γ front in the specimen heated for 8 s at 800°C. The SAED pattern taken from the untransformed pearlite [Fig. 6(c)] shows that the ferrite and the cementite obey the Pitsch–Petch OR with the habit plane of $(001)_C//(512)_F$. Figures 6(d) and (e) are the SAED patterns taken from the different transformed regions. Three martensite orientations were recognized. The incident beam is $[\bar{3}55]_F//[135]_{M1}//[\bar{1}\bar{3}\bar{5}]_{M2}//[\bar{2}3\bar{1}]_{M3}$. The stereographic analysis [Fig. 6(f)] shows that martensite crystals 1 and 2 are twin related as far as the ORs are concerned and the orientation of martensite crystal 3 is close to that of crystal 1. All of them exhibit the Bagaryatsky OR [27] with cementite. The habit plane between the cementite lamellae and adjacent martensites can be expressed as follows:

$$(001)_C//(1\bar{2}1)_{M1}//(1\bar{2}1)_{M2}//(21\bar{1})_{M3}.$$

Despite the fact that the austenite is never retained in our experiments, its orientation can be deduced by assuming the austenite/martensite OR so far obtained. It is well established that austenite transforms to martensite via either the Kurdjumov–Sachs [28] or the Nishiyama–Wasserman OR [29, 30]. If the twin-related sets of martensite are assumed to arise from a parent austenite with the Kurdjumov–Sachs OR between the austenite and martensite, the Pitsch OR [19] between the austenite and cementite will be reached within a few degrees as shown in the stereographic projection. In such a situation, the habit plane of cementite lamellae is preserved during the $\alpha \longrightarrow \gamma \longrightarrow \alpha'$ transformation

$$(001)_C//(512)_F//(52\bar{2})_A//\{112\}_M.$$

Similar conclusions can be obtained from the stereographic analysis presented in Fig. 7(d). Figure 7(a) shows the α/γ front (austenite transformed into martensite during subsequent quenching). Cementite lamellae remained almost undissolved in the region close to the α/γ front. Figures 7(b) and (c) are the SAED patterns taken from the ferrite/cementite and the martensite/cementite regions, respectively. Assuming that the martensite is related to the austenite by the Kurdjumov–Sachs OR, the following ORs among the coexisting phases can be deduced.

The ferrite relates to the cementite by the Pitsch–Petch OR:

$$(00\bar{1})_C//(5\bar{2}1)_F\text{-habit plane},\ (100)_C//(131)_F,$$

$$(0\bar{1}0)_C//(\bar{1}\bar{1}3)_F.$$

The martensite relates to the cementite by the Bagaryatsky OR:

$$(00\bar{1})_C//(\bar{1}\bar{2}1)_M\text{-habit plane},\ (100)_C//(101)_M,$$

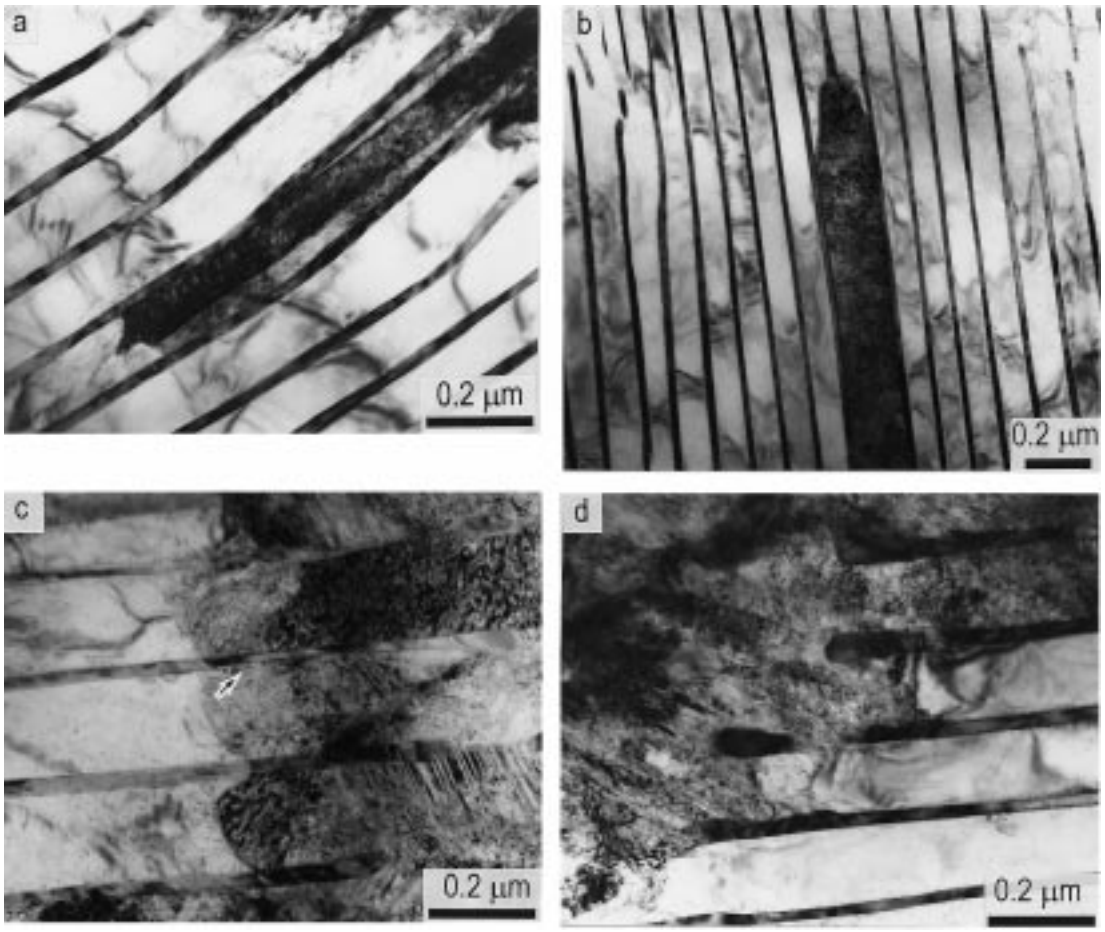

Fig. 4. TEM micrographs showing α/γ fronts (austenite completely transformed into martensite during quenching) after heat treatment at 800°C for various times: (a) 8 s; (b) 20 s; (c) 10 s; (d) 20 s.

$$(0\bar{1}0)_C//(\bar{1}11)_M.$$

The cementite relates to the austenite by the Pitsch OR:

$$(00\bar{1})_C//(2\bar{2}5)_A\text{-habit plane},\ (100)_C//(5\bar{5}\bar{4})_A,$$

$$(0\bar{1}0)_C//(110)_A.$$

The austenite relates to the martensite by the Kurdjumov–Sachs OR:

$$(\bar{1}11)_M//(110)_A,\ (101)_M//(1\bar{1}\bar{1})_A,\ (\bar{1}\bar{2}1)_M//(1\bar{1}2)_A.$$

In such a situation, the austenite/ferrite orientation relationship will be rather far from that of either Kurdjumov–Sachs or Nishiyama–Wasserman. The ORs described above can be deduced at least in five cases when one or several martensite crystals were related to the cementite by the Bagaryatsky OR.

A crystallographic relationship between the growing austenite and both pearlite constituents was examined further. Figure 8 shows the α/γ front within the pearlite obeying the Pitsch–Petch OR. Two main martensite orientations were recognized, but neither of them has any rational OR with cementite. It was also found that the martensite orientations observed could never satisfy any variants of both the Kurdjumov–Sachs and the Nishiyama–Wasserman ORs with austenite assuming the Pitsch OR between the austenite and the cementite. The ORs between Widmanstätten cementite and austenite reported by Farooque–Edmonds [31] and Zhang–Kelly [32] would yield neither of the observed martensite orientations on transformation of austenite into martensite with the OR so far obtained. Thus, it can be concluded that the austenite had no reproducible OR with respect to the cementite. Similar conclusions were obtained in many other cases. Dippenaar and Honeycombe [33] reported for pearlite possessing the Pitsch–Petch OR that the pearlitic ferrite and cementite were related to the austenite grain into which it was not growing. It is obvious from Fig. 1 that such an OR was not obeyed during the reverse transformation.

Up to here the existence of a specific OR between austenite and cementite was assumed. However, the possibility that the austenite is related to the pearlitic ferrite should also be considered. Fong and Glover [34] showed that the grain boundary austenite precipitates were related to at least one of the

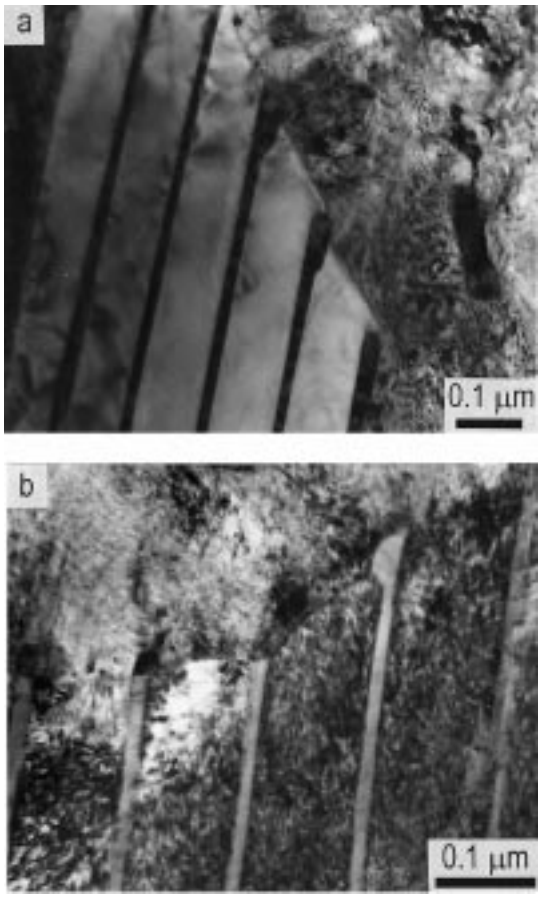

Fig. 5. TEM micrographs showing various stages of an $\alpha \longrightarrow \gamma$ transformation in the two adjacent pearlite colonies after heat treatment: (a) at 800°C for 20 s; (b) at 875°C for 3 s.

ferrite grains at the nucleating grain boundary by the Kurdjumov–Sachs OR within 15°. The stereographic projection in Fig. 8(e) shows a combination of the Kurdjumov–Sachs ORs between pearlitic ferrite and austenite and between austenite and either martensite that could be observed within 6°. In this case any rational OR between austenite and cementite could not be found. It should be emphasized that a similar sequence of the Kurdjumov–Sachs ORs during the $\alpha \longrightarrow \gamma \longrightarrow \alpha'$ transformation could not be observed in the case presented in Fig. 6. Thus, the austenite had no reproducible OR with respect to the pearlitic ferrite although both phases can occasionally be related by the Kurdjumov–Sachs OR. This finding agrees well with results of Law and Edmonds [11] who showed that the orientation of austenite growing in the ferrite was away from an exact Kurdjumov–Sachs OR. They also confirmed the hypothesis of Smith [14] that the austenite allotriomorphs nucleated on a ferrite grain boundary bear a Kurdjumov–Sachs OR to one ferrite grain, and grow into the adjacent grain by migration of an incoherent interface. In the present study the shape of the α/γ was often observed to be irrational [Fig. 4(a)], suggesting the advancing of an incoherent interface. Finally, it should be pointed out that, in the case of pearlite growth, any reproducible OR between pearlite and its parent phase has also not been observed [33, 35].

4. DISCUSSION

4.1. Summary of the experimental results

In the present study, the crystallography and the microstructure evolution of pearlite during $\alpha \longrightarrow \gamma \longrightarrow \alpha'$ transformation were studied. The experimental observations described above can be summarized as follows.

1. Although austenite grains nucleated after 8 s at 800°C, the reaction was not completely finished even after 20 s. At 875°C full austenitization was completed within 3 s.
2. Nucleation of austenite in pearlite occurred mainly at the pearlite colony boundaries. Austenite grains also nucleated at the ferrite/cementite interfaces within a pearlite colony. Such a nucleation was observed both at the beginning and at the end of the $\alpha \longrightarrow \gamma$ transformation (Figs 3 and 6).
3. Various shapes of the α/γ interface were observed, i.e. almost flat, concave, convex or even in corrugated shapes.
4. The austenite grains nucleated at a pearlite colony boundary grew into one of the adjacent grains preferentially by the migration of an incoherent interface. The possible austenite orientations were evaluated from the orientations of several martensite crystals assuming the austenite/cementite and austenite/martensite ORs so far obtained. It was shown that there are no reproducible ORs between austenite and pearlitic constituents on both sides of the grain boundary. Meanwhile, in some cases where the pearlite exhibited the Pitsch–Petch OR, the austenite could be related either with cementite by the Pitsch OR or with ferrite by the Kurdjumov–Sachs OR.
5. Some pearlite colonies remained completely untransformed even after the $\alpha \longrightarrow \gamma$ transformation in the other grains was completed.
6. Various cementite morphologies in the vicinity of the α/γ interface were observed:

   (a) cementite lamellae remained almost undissolved behind the moving α/γ interface [Figs 4(a), (b) and 7];

   (b) cementite lamellae dissolved completely [Fig. 4(d)];

   (c) rows of cementite particles aligned behind the dissolved lamella (Fig. 8).

7. Edgewise cementite dissolution was predominant. Thickening and spheroidization of the edges of

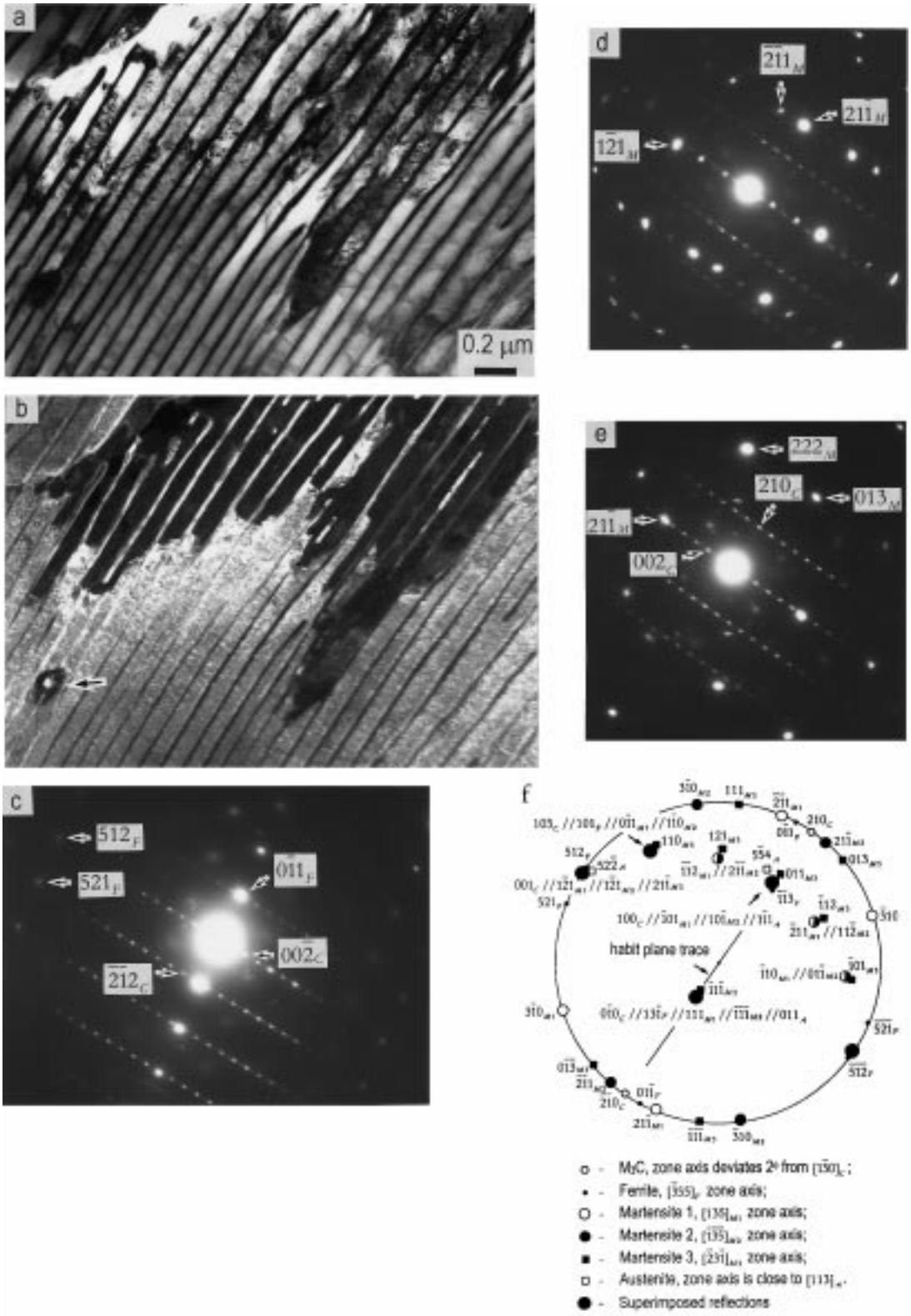

Fig. 6. (a) Bright field image and (b) dark field image using the $0\bar{1}1$ ferrite reflection showing an α/γ front (austenite completely transformed into martensite during quenching) after heat treatment at 800°C for 8 s. Arrow shows the nucleation of austenite at the ferrite/cementite interface within pearlite. (c) SAED pattern taken from the initial pearlite. (d), (e) SAED patterns taken from the different areas behind the α/γ front. (f) The $[\bar{3}55]_F//[135]_{M1}//[\bar{1}\bar{3}\bar{5}]_{M2}//[\bar{2}3\bar{1}]_{M3} \approx //[1\bar{3}0]_C \approx //[113]_A$ stereographic projection showing the habit plane and the OR between coexisting phases during the $\alpha \longrightarrow \gamma \longrightarrow \alpha'$ transformation.

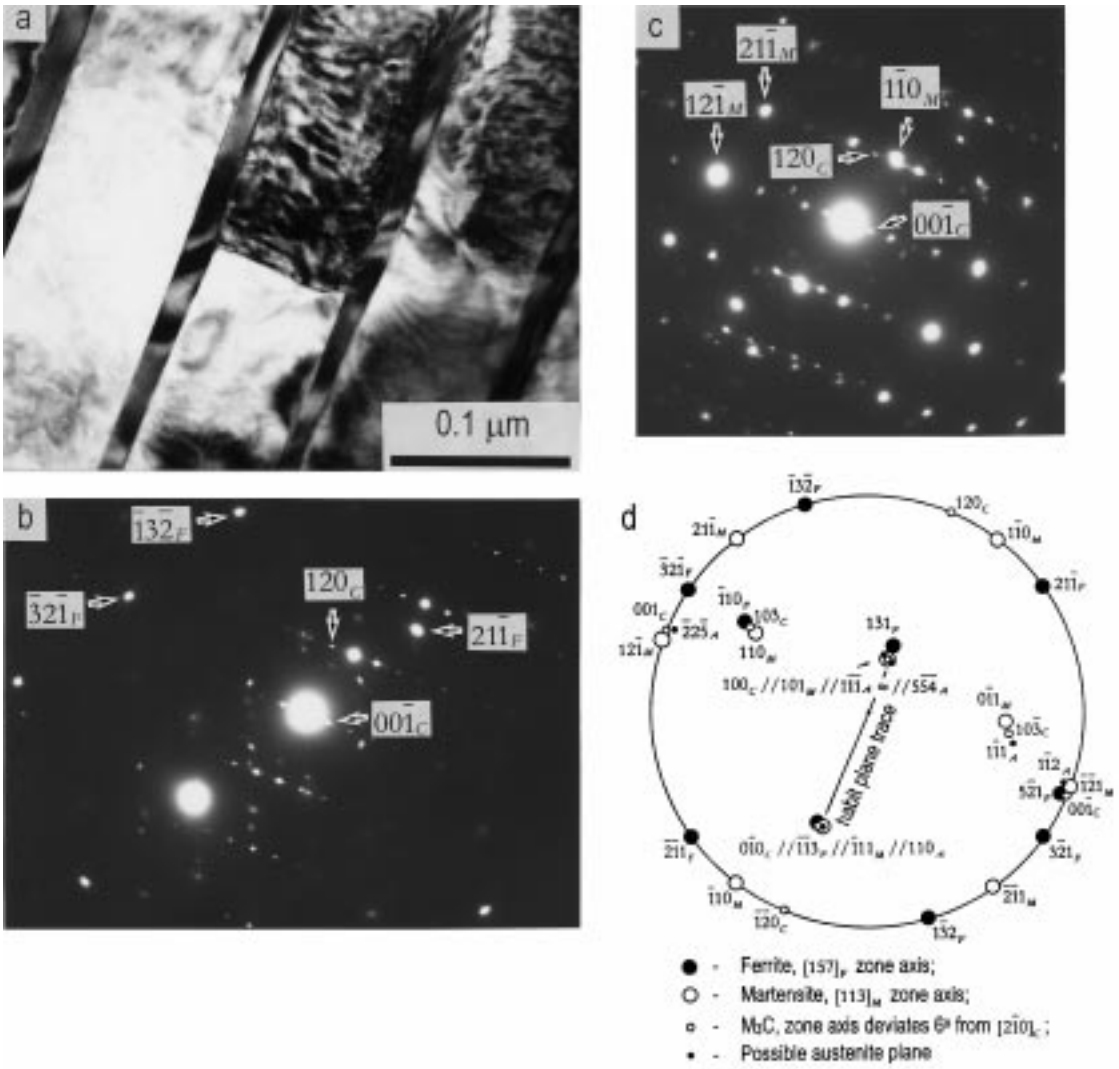

Fig. 7. (a) TEM micrograph showing an α/γ front (austenite completely transformed into martensite during quenching) after heat treatment at 800°C for 20 s. (b), (c) SAED patterns taken from the ferrite/cementite and martensite/cementite regions, respectively. (d) Stereographic analysis.

the cementite lamellae both at the α/γ front and behind it were frequently observed.

8. The morphology of martensite after $\alpha \longrightarrow \gamma \longrightarrow \alpha'$ transformation indicates that the growing austenite could be of either low or high carbon content.
9. In the case of the pearlite exhibiting the Pitsch–Petch OR, the martensite crystals, which finally formed after $\alpha \longrightarrow \gamma \longrightarrow \alpha'$ transformation, were often related to cementite with the Bagaryatsky OR. They were often found to be twin related. In the case of the Isaichev OR, any rational OR between martensite and cementite was not found.

From the results obtained, it can be concluded that the austenitization of alloyed pearlite occurs via various complicated processes and various kinetics of austenite growth can be expected. The structural evolution in the Fe–2.6Cr–0.96C alloy is much closer to that in the Fe–8Cr–C alloy [16] than in plain carbon steel [1]. This is probably due to the presence of the carbide stabilizing elements such as chromium. The results are summarized in Table 2.

4.2. *Theoretical consideration*

When the formation of austenite is considered, it is expected that the reaction will be controlled either by a fast diffusion of carbon or by a slow diffusion of substitutional alloying elements. Despite the large difference in the mobility between carbon and substitutional elements like Cr, the reaction is not always controlled by carbon diffusion. In order to find the thermodynamic driving forces for diffusion, the activities at all moving interfaces should be thoroughly established. It is thus useful to examine the corresponding phase diagrams. In the pre-

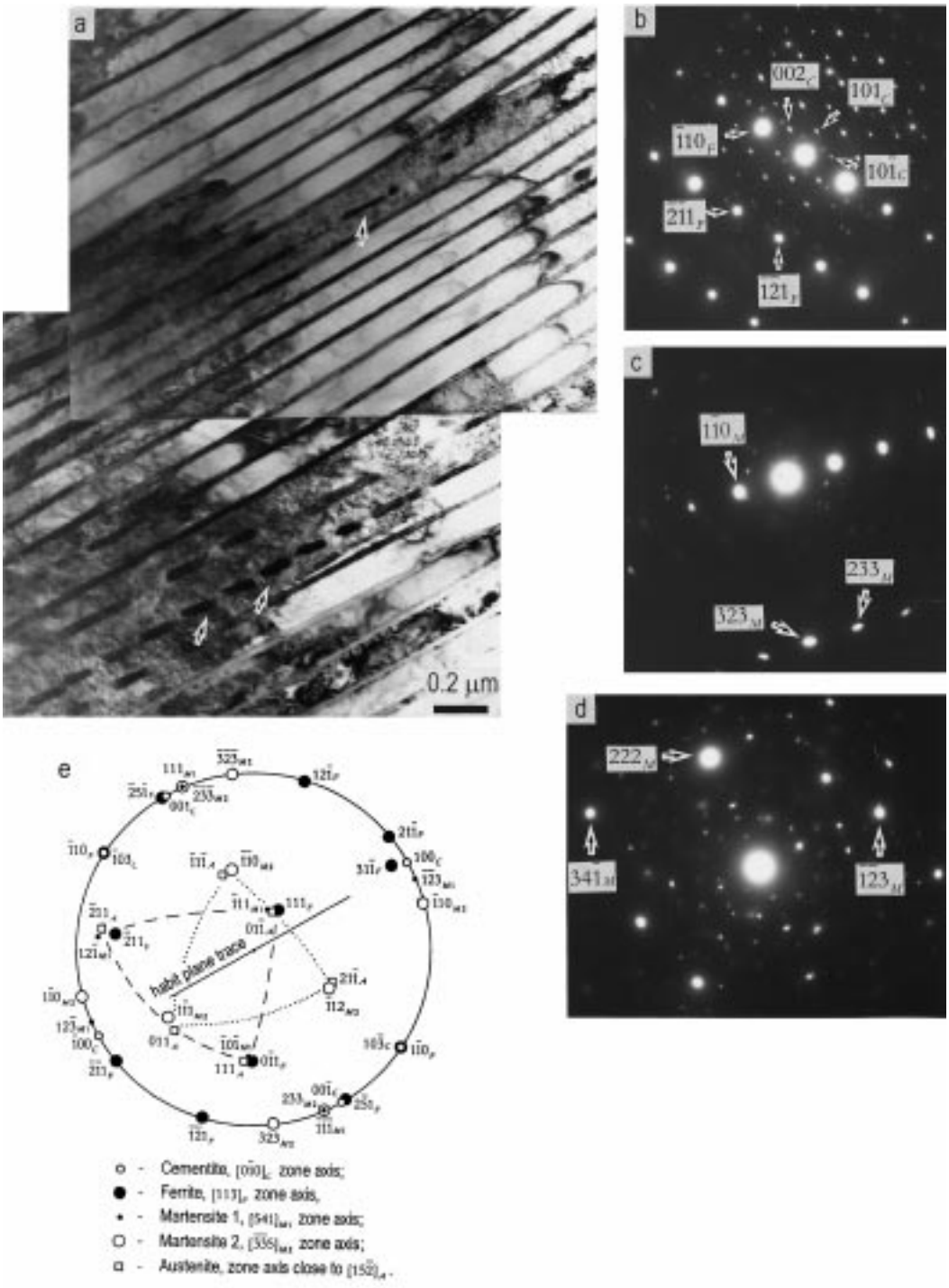

Fig. 8. (a) TEM micrograph showing an α/γ front (austenite completely transformed into martensite during quenching) after heat treatment at 800°C for 20 s. (b) SAED pattern showing that the initial pearlite possesses the Pitsch–Petch OR. (c), (d) SAED patterns taken from the different martensites behind the α/γ front. (e) Stereographic analysis.

sent treatment, local equilibrium is assumed at the phase interfaces. This hypothesis has been applied for the explanation of various complicated reactions [16, 37, 38] and the experiments appear to be in agreement with theories.

Figure 9 shows calculated isothermal sections of the Fe–Cr–C phase diagram at 800°C, representing the metastable $\alpha + \gamma + M_3C$ three-phase equilibrium with different axes. Since the precipitation of M_7C_3 stable carbide was not observed during the reaction,

Table 2. Characteristics of pearlite to austenite transformation in different alloys

Plain carbon steel (α + M_3C pearlite)	Fe–2.6Cr–0.96C alloy (α + M_3C pearlite)	Fe–8.2Cr–0.2C alloy (α + $M_{23}C_6$ pearlite) [16]	Fe–8.2Cr–0.96C alloy (α + M_7C_3 pearlite) [16]
1. The nucleation of austenite occurs instantaneously without any nucleation barrier [1, 5]	Austenite nucleates after rather long incubation times:		
	8 s at 800°C	2 s at 870°C	20, 8 and 3 s at 850, 870 and 900°C, respectively
2. Austenite nucleates at a pearlite colony boundary [1, 4, 5]	Austenite nucleates both at the pearlite grain boundaries and at the ferrite/carbide interface within pearlite		Austenite nucleates at the pearlite grain boundaries
3. Nucleation of austenite is not a rate-limiting factor for the complete austenitization [5]	Nucleation of austenite is a rate-limiting factor for the complete austenitization		
4. α/γ interface is considerably bowed [1]; α/γ interface can be flat or curved [36]	Flat, convex and concave α/γ interfaces are observed		
5. Growth of the austenite is controlled by carbon diffusion in austenite [1, 5]	The kinetics of austenite growth changes from the carbon diffusion controlled to chromium diffusion controlled	Growth of the austenite is controlled by chromium diffusion	The kinetics of austenite growth changes from the carbon diffusion controlled to chromium diffusion controlled
6. Thin parts of cementite lamellae remain behind the α/γ interface [38]; the thickness of cementite lamellae decreases gradually behind the α/γ interface [2]; the residual carbide particles dissolve completely or spheroidize behind the α/γ interface [1]	Various carbide morphologies are observed: (a) carbide lamellae remain almost undissolved; (b) carbide lamellae dissolve completely; (c) carbide lamellae thicken and spheroidize just at the α/γ interface		

it was excluded. The dotted lines show calculated metastable extensions of the $\alpha + M_3C$ and $\gamma + M_3C$ two-phase equilibria. The open square (□) denotes the composition of the alloy investigated. The initial composition of pearlitic cementite formed during continuous cooling from the austenite region is represented by a cross (+). The open circle (○) represents the composition of the initial pearlitic ferrite. This composition is equal to the solubility limit for carbon in ferrite at 650°C. The diagram shows that the composition of the initial ferrite falls inside the α single-phase field at 800°C, indicating that the pearlitic ferrite is stable at this temperature. At higher temperature, the solubility limit shifts to higher carbon content. At the austenitizing temperature under consideration, the solubility limit is obtained as the intersection of the tie-line starting from the cross (+) with the metastable extension of the $\alpha + M_3C$ boundary [shown in the magnified diagram in Fig. 9(b) by a filled circle (●)]. The carbon activity difference $\Delta a = a^2 - a^1$ [Fig. 9(c)] between the α/M_3C interface (●) and the bulk α (○) produces an initial driving force for carbon diffusion. This reaction is completed very rapidly and the carbon activity becomes uniform within the material. During Stage 1 the carbon content in the ferrite slightly changes, and then the composition of the ferrite falls well inside the $\alpha + \gamma$ two-phase field close to the α-phase boundary [(●) in Fig. 9(b) inset] meeting thermodynamic requirements for the austenite nucleation.

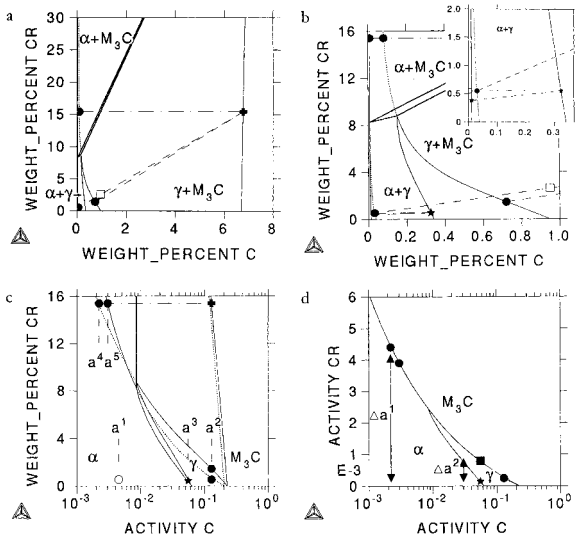

Fig. 9. Calculated isothermal section of the Fe–Cr–C phase diagram at 800°C representing the metastable $\alpha + \gamma + M_3C$ three-phase equilibruum with (a) and (b) weight percent carbon and (c) and (d) carbon activity as horizontal axes. The dotted lines show calculated metastable extensions of $\alpha + M_3C$ and $\gamma + M_3C$ two-phase equilibria. The slanting dashed lines represent the tie-lines of the $\alpha + M_3C$, $\gamma + M_3C$ and $\alpha + \gamma$ equilibria. The horizontal dash-dotted lines define the compositions of γ phase if it inherits the chromium contents of the α or M_3C. The composition of alloy is marked by (□). All the other symbols are explained in Section 4.2.

In view of the high mobility of carbon in comparison with chromium, the possibility of a reaction without partitioning of chromium has to be considered first. At such a situation the austenite inherits the chromium content from the ferrite [as shown by horizontal dash-dotted line in Fig. 9(b) inset]. The composition of ferrite at the α/γ interface is thus given by the tie-line joining two stars (★) in

the inset in Fig. 9(b). The corresponding carbon activity at the α/γ interface can be seen in Fig. 9(c) as a^3. Since the composition of cementite does not change during the first stage the two tie-lines starting from the cross (+) define the compositions of α and γ at the α/M_3C and γ/M_3C interfaces [Figs 9(a) and (b)]. The carbon activities at both the interfaces are defined by the isoactivity line a^2 [Fig. 9(c)]. Thus the carbon activity difference $\Delta a = a^2 - a^3$ produces the driving force for carbon diffusion from the α/M_3C and γ/M_3C interfaces toward the α/γ interface, resulting in the interface migration.

At present, the role of carbon diffusion ahead of the moving α/γ interface is unknown. Speich and Richards [1] excluded this process from their theoretical consideration, while Hillert *et al.* [2] objected to their interpretation. They noted that during the growth of pearlite the diffusion processes ahead of the advancing interface are of great importance and there are no reasons to neglect them during the reverse transformation. Note that our experimental observation did not reveal any shrinkage of cementite lamellae ahead of the α/γ interface whereas behind it cementite lamellae can dissolve in a great extent. The problem will be discussed below in more detail. For the sake of argument, in a first approximation, we neglect the carbon diffusion in ferrite ahead of the α/γ interface.

Figure 10 shows schematically various stages of the austenite growth reaction. When austenite nucleates at a pearlite colony boundary, carbon diffuses away from the α/M_3C interface toward the α/γ interface [Fig. 10(a)]. Carbon atoms diffuse into the austenite matrix very rapidly in comparison with chromium atoms and the austenite will inherit the chromium content from dissolved cementite [marked by γ^* in Fig. 10(b)]. From the experimental observation, it can be concluded that the edgewise cementite dissolution is the predominant process in comparison with the sidewise dissolution. The solubility limit for carbon within γ^* is given by the intersection of the γ/M_3C boundary with the line of constant chromium content starting from the cross (+) [Figs 9(a) and (b)]. It can be seen in Fig. 9(c) that the activity of carbon at the γ^*/M_3C interface shifts to the very low value of a^4, building up the carbon activity difference $\Delta a = a^2 - a^4$ between the γ/M_3C and γ^*/M_3C interfaces. Carbon atoms diffuse toward the edge of cementite lamella [Fig. 10(b)] resulting in lamella thickening and spheroidization just behind the moving α/γ interface (see Fig. 4). The subsequent advancement of the α/γ front controlled by carbon diffusion is possible only by the sidewise carbide dissolution. Diffusion of carbon from the γ/M_3C interface toward the both γ^*/M_3C and α/γ interfaces will produce a row of cementite particles aligning behind the edge of carbide lamella [Figs 10(c) and 8].

If the cementite lamellae dissolved considerably behind the α/γ interface as shown in Figs 10(d) and (e), the growth of austenite controlled by carbon diffusion in austenite would slow down and eventually stop since the carbon activity difference $\Delta a = a^2 - a^4$ drives the diffusion of carbon in the opposite direction. The $\alpha \longrightarrow \gamma$ transformation will proceed only if the chromium diffusion in the vicinity

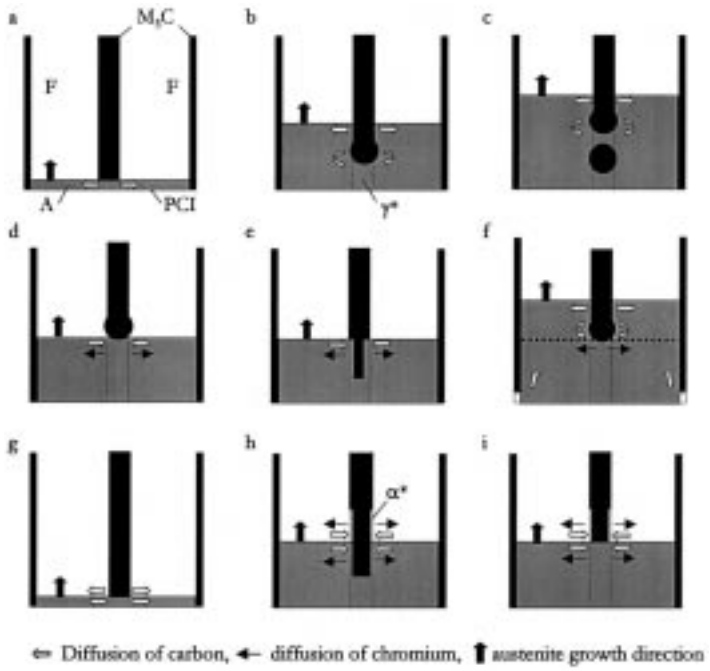

Fig. 10. Various stages of the austenite growth reaction (schematic) in the lamellar pearlite. PCI indicates the intersection of pearlite colonies. α^* and γ^* denote the ferrite and austenite with the chromium compositions inherited from the dissolved cementite lamella.

of the α/γ interface occurs. This is regarded as Stage 3. It is important to note that Stage 3 can be delayed if additional carbon atoms diffuse from the bulk austenite toward the α/γ interface as shown in Fig. 10(f) and the situation becomes similar to that presented in Fig. 10(c).

At the end of the carbon-controlled reaction (Stage 2), the carbon activity has to be uniform within the material because of the larger diffusivity of carbon in comparison with chromium. Thus the value close to a^3 is expected to establish at all three interfaces during Stage 3. Figure 9(d) shows how the chromium activity difference between the γ/M_3C and α/γ interfaces changes during the reaction controlled by chromium diffusion from Δa^1 to Δa^2.

From the experimental observation it is inferred that the cementite lamellae acted as barriers for the sidewise growth of austenite and carbon diffusion. Thus it is expected that Stage 2 is not completed simultaneously within the whole material, some parts of a pearlite will transform to austenite via a carbon diffusion-controlled reaction whereas in other parts of a pearlite the reaction is already controlled by chromium diffusion. Note that the possibility of the redistribution of chromium by the interface diffusion cannot be excluded.

Now the diffusion of carbon atoms ahead of the α/γ interface will be discussed. Similar to the diffusion of carbon in austenite, the carbon activity difference $\Delta a = a^2 - a^3$ [Fig. 9(c)] produces the driving force for carbon diffusion between the α/M_3C interface and the α/γ interface [Fig. 10(g)]. The dissolution of carbide lamellae just ahead of the α/γ interface results in the formation of ferrite with the chromium content inherited from the cementite (shown as α^*). The activity of carbon at the α/γ interface changes drastically from a^2 to a^5 [Fig. 9(c)] and the diffusion of carbon changes into the opposite direction as shown in Figs 10(h) and (i). Thus Stage 2 should be completed more rapidly.

Shtansky and Inden [37] first presented the experimental evidence that the diffusion of carbon in ferrite at austenitizing temperatures is of great importance. They showed that the $M_{23}C_6$ carbide particles may be dissolved up to 25 vol.% in contact with ferrite at temperatures within the range of 800–900°C. In the present study any experimental evidence of the cementite dissolution in contact with ferrite has not been found. Nevertheless it should be emphasized that we did not find any experimental indications showing a significant role of either carbon or chromium diffusion just ahead of the α/γ front.

Up to here the formation of austenite at a pearlite colony boundary was considered. The possibility of austenite nucleation at an α/M_3C interface within a pearlite has been discussed by Speich and Szirmae [1], but this reaction has not been confirmed experimentally. They proposed that there is no low energy γ/M_3C interface. On the contrary, the nucleation of austenite at the $\alpha/M_{23}C_6$ interface has been experimentally confirmed by Shtansky *et al.* [16]. They explained the observed orientations of twin martensite crystals assumed the parallel OR between $M_{23}C_6$ carbide and austenite.

In the present study, the nucleation of austenite at the α/M_3C interface within pearlite was also observed. As was shown in Section 3.4, it can be assumed that at least in some cases the cementite and austenite are related by the Pitsch OR. Despite the fact that in this case the γ/M_3C interface is semicoherent, its interface energy is probably very high. Spanos and Aaronson [39] showed that the $(\bar{1}13)_A//(001)_C$ habit plane in the case of the Pitsch–Petch OR between pearlitic constituents gives a good match in only one direction normal to the "good fit" direction $[110]_A//[010]_C$, whereas $(\bar{2}25)_A//(001)_C$ yields no matching at all. They showed that only $(1\bar{1}3)_A//(101)_C$ exhibits a superior matching. The new OR with the habit plane $(\bar{4}21)_A//(015)_C$ has recently been reported by Zhang and Kelly [32]. It is apparently that either of them cannot be fulfilled during the austenitization of pearlite.

Finally, it should be noted that this is a qualitative approach to an extremely complicated problem in kinetics and can therefore be expected to provide only a first approximation to the reverse transformation of an alloyed pearlite.

4.3. Sidewise dissolution of cementite lamellae

From a theoretical point of view, it is important to know whether carbon and substitutional atoms diffuse in the α-phase ahead of the α/γ front. Another question remaining to be addressed and clarified is whether cementite lamellae can remain almost undissolved just behind the α/γ interface as it is often inferred from the experimental observation. The determination of the boundary conditions close to the α/γ front is very important because the activity differences between these interfaces would act as a driving force for the diffusion. Figure 11(a) shows an α/γ front in the specimen heated for 9 s at 800°C. The austenite advancing between the adjacent cementite lamellae which seem almost undissolved in the region close to the α/γ interface. A lattice image is from (001) cementite planes, which is the broad face on the habit plane. The cementite habit plane deviates about 2° from $(001)_C$.

It is rather difficult to analyze whether cementite shrunk or not by the sidewise dissolution because the ferrite/cementite interface is not always straight. The ledges are frequently observed on both sides of the broad face of the cementite lamella [40]. In the case under consideration, the left lamella is straight without any steps [Fig. 11(b)]. The steps shown by small arrows on both sides of the right lamella indicate the directions of the initial cementite growth. These steps may accommodate the deviation of the

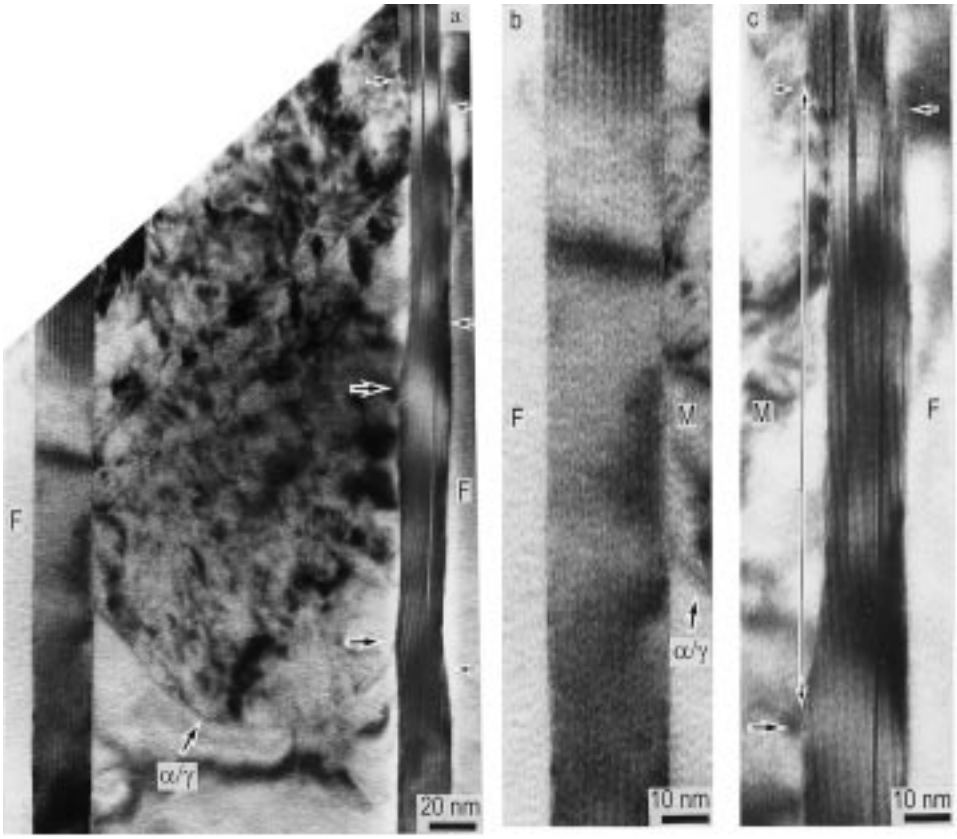

Fig. 11. (a)–(c) TEM micrographs showing the sidewise dissolution of a cementite lamella. The α/γ front (austenite completely transformed into martensite during quenching) after heat treatment at 800°C for 9 s. (b), (c) The left and right lamellae shown in (a) at higher magnification. The small arrows indicate the direction steps on the broad face of the cementite lamella. The large arrows show the remaining parts of the growth ledge after the sidewise cementite dissolution.

habit plane from the $(001)_C$. No modifications in the structure of the ferrite/cementite interfaces ahead of the α/γ front were observed. The dissolution of cementite can hardly be recognized in the left lamella behind the α/γ interface, and the interface is almost straight [see Fig. 11(b)]. A small step at the α/γ interface which is equal to one unit lattice height of cementite in the $[001]_C$ direction can be attributed to the initial growth ledge. On the right lamella the two risers (shown by large arrows) can be observed between the α/γ interface and the large step located 0.23 μm behind it. A part of the lamella between the large step and the first riser at a higher magnification is shown in Fig. 11(c). The height of the riser is equal to that of the step, i.e. six unit lattice height of $(001)_C$ cementite planes. Thus the part of cementite between these risers probably dissolved during the reaction. The part of the interface between the first and second risers is also concave suggesting the sidewise lamella dissolution. These results will support the assumption that the local equilibrium conditions are varied at the austenite/cementite interface behind the α/γ front depending on the extent of the sidewise cementite dissolution.

5. SUMMARY

The mechanism of austenite formation, the kinetics of cementite lamellae dissolution and the crystallography during the reverse transformation of pearlite have been studied in an Fe–2.6 wt% Cr–0.96 wt% C alloy. The following results were obtained.

1. Austenite nucleated after the incubation time, 8 s at 800°C. Two types of nucleation have been distinguished: at a pearlite grain boundary and at a ferrite/cementite interface within a pearlite.
2. The austenite nucleated at a pearlite colony boundary grew only into one of the adjacent grains and did not cross the pearlite colony boundary in the opposite grain.
3. Various cementite morphologies were observed close to the α/γ interface and can be explained by the kinetics. The edgewise cementite dissol-

ution was the predominant process in comparison with the sidewise dissolution.
4. The kinetics of austenite growth changed from carbon diffusion controlled to chromium diffusion controlled.
5. The structural evolution in the specimen close to the α/γ interface has been thoroughly studied. No indications of either carbon or chromium diffusion ahead of the α/γ interface have been found.
6. Phase transformation theory applicable to the determination of the driving force for diffusion has been developed. The structural evolution during the reaction can be qualitatively understood by assuming the local equilibrium at the interfaces. This approach predicts that the local equilibrium conditions are varied at the austenite/cementite interface behind the α/γ front depending on the sidewise cementite dissolution.
7. The crystallography between coexisting phases during the $\alpha \longrightarrow \gamma \longrightarrow \alpha'$ transformation has been determined. The possible austenite orientations were evaluated assuming the orientation relationships so far obtained. Although the austenite could not have any reproducible OR with respect to either of the pearlite constituents, in the case of pearlite with the Pitsch–Petch OR the austenite could occasionally be related either with cementite by the Pitsch OR or with ferrite by the Kurdjumov–Sachs OR. In the case of pearlite with the Pitsch–Petch OR the martensites were often related to cementite by the Bagaryatsky OR whereas in the case of the Isaichev OR no rational OR has been found.

Acknowledgements—D.S. acknowledges the support of the Japan Society for the Promotion of Science during the work. This research was supported by the Grant-in-Aid of The Ministry of Education, Science, Culture and Sports. Thanks are also due to Sumitomo Metal Industries for supplying the materials used in the present study.

REFERENCES

1. Speich, G. R. and Szirmae, A., *Trans. metall. Soc. A.I.M.E.*, 1969, **245**, 1074 (with Appendix by Spech, G. R. and Richards, M. J.).
2. Hillert, M., Nilsson, K. and Törndahl, L.-E., *J. Iron Steel Inst.*, 1971, **209**, 49.
3. Datta, D. P. and Gokhale, A. M., *Metall. Trans. A*, 1981, **12A**, 443.
4. Garcia, C. I. and Deardo, A. J., *Metall. Trans. A*, 1981, **12A**, 521.
5. Speich, G. R., Demarest, V. A. and Miller, R. L., *Metall. Trans. A*, 1981, **12A**, 1419.
6. Souza, M. M., Guimarães, J. R. C. and Chawla, K. K., *Metall. Trans. A*, 1982, **13A**, 575.
7. Yang, D. Z., Brown, E. L., Matlock, D. K. and Krauss, G., *Metall. Trans. A*, 1985, **16A**, 1385.
8. Yi, J. J., Kim, I. S. and Choi, H. S., *Metall. Trans. A*, 1985, **16A**, 1237.
9. Navara, E., Bengtsson, B. and Easterling, K. E., *Mater. Sci. Technol.*, 1986, **2**, 1196.
10. Goel, N. C., Chakravarty, J. P. and Tangri, K., *Metall. Trans. A*, 1987, **18A**, 5.
11. Law, N. C. and Edmonds, D. V., *Metall. Trans. A*, 1980, **11A**, 33.
12. Jayaswal, S. K. and Gupta, S. P., *Z. Metallk.*, 1992, **83**, 809.
13. Gupta, S. P. and Yadav, K., *Z. Metallk.*, 1998, **89**, 222.
14. Smith, C. S., *Trans. Am. Soc. Metals*, 1953, **45**, 533.
15. King, A. D. and Bell, T., *Metall. Trans. A*, 1975, **6A**, 1419.
16. Shtansky, D. V., Nakai, K. and Ohmori, Y., *Z. Metallk.*, 1999, **90**, 25.
17. Zhang, M.-X. and Kelly, P. M., *Scripta mater.*, 1997, **37**, 2009.
18. Petch, N. J., *Acta crystallogr.*, 1953, **6**, 96.
19. Pitsch, W., *Acta metall.*, 1962, **10**, 897.
20. Zhou, D. S. and Shiflet, G. J., *Metall. Trans.*, 1992, **23A**, 1259.
21. Isaichev, I. V., *Zh. tekh. Fiz.*, 1947, **17**, 835.
22. Sukhomlin, G. D., *Fizika Metall.*, 1976, **42**, 965.
23. Ridley, N., *Proc. Int. Conf. on Phase Transformation in Ferrous Alloys*, October 1983, Philadelphia, PA, ed. A. R. Marder and J. I. Goldstein. TMS–AIME, Warrendale, PA, 1984, p. 201.
24. Baker, A., Kelly, P. M. and Nutting, J., *Electron Microscopy and Strength of Crystals*. Interscience, NY 1961, p. 899.
25. Darken, L. S. and Fisher, R. M., *Decomposition of Austenite by Diffusional Processes*. Interscience, NY 1962, p. 249.
26. Sundman, B., Jansson, B. and Andersson, J.-O., *CALPHAD*, 1985, **9**, 153.
27. Bagaryatsky, Y. A., *Dokl. Akad. Nauk SSSR*, 1950, **73**, 1161.
28. Kurdjumov, G. V. and Sachs, G., *Z. Phys.*, 1930, **64**, 325.
29. Nishiyama, Z., *Sci. Rep. Tohoku Univ.*, 1934, **23**, 637.
30. Wasserman, G., *Arch. Eisenhutt Wes.*, 1933, **16**, 647.
31. Farooque, M. and Edmonds, D. V., *Proceedings of the XIIth Int. Congress for Electron Microscopy*, San Francisco, 1990, p. 910.
32. Zhang, M.-X. and Kelly, P. M., *Acta mater.*, 1998, **46**, 4617.
33. Dippenaar, R. J. and Honeycombe, R. W. K., *Proc. R. Soc. Lond. A*, 1973, **333**, 455.
34. Fong, H. S. and Glover, S. G., *Trans. Japan Inst. Metals*, 1975, **16**, 115.
35. Hackney, S. A. and Shiflet, G. J., *Acta metall.*, 1987, **5**, 1007.
36. Nemoto, M., *Metall. Trans.*, 1977, **8A**, 431.
37. Shtansky, D. V. and Inden, G., *Acta mater.*, 1997, **45**, 2879.
38. Shtansky, D. V., Nakai, K. and Ohmori, Y., *Phil. Mag. A*, in press.
39. Spanos, G. and Aaronson, H. I., *Acta metall. mater.*, 1990, **38**, 2721.
40. Zhou, D. S. and Shiflet, G. J., *Metall. Trans. A*, 1991, **22A**, 1349.